Progress In Electromagnetics Research Letters, Vol. 98, 17–24, 2021

Orbital Angular Momentum Orthogonality Based Crosstalk Reduction

Unaiza Tariq*, Hiva Shahoei, Guang Yang, and Duncan L. MacFarlane

Abstract—We report a reduction in crosstalk between a transmitting antenna and an adjacent receiving antenna due to the use of radiation patterns with different orbital angular momentum (OAM). This crosstalk reduction is based on the orthogonality between different OAM modes. To generate OAM beams, patch array antennas are designed using High frequency simulation software (HFSS). The designed antennas are fabricated and characterized. An experiment is carried out to determine the amount of crosstalk reduction achieved due to the OAM nature of the signals transmitted. The variation of this crosstalk reduction with the distance between the transmitting and receiving antennas is also studied. The results obtained are verified through theoretical analysis using simulations in HFSS. A maximum theoretical crosstalk reduction of 3.6 dB has been obtained, and a crosstalk reduction of 2.6 dB has been realized experimentally. The results may benefit full-duplex communication links.

1. INTRODUCTION

It is known from Maxwell's theory that electromagnetic radiation carries not only energy but also momentum. The angular part can be divided into two types, spin momentum and orbital momentum. Spin momentum determines the polarization, whereas orbital angular momentum is associated with spatial distribution [1]. Unlike spin angular momentum, electromagnetic waves carrying OAM can have theoretically infinite orthogonal states. This quality is highly desirable in the field of communication; over the last two decades, the characteristics and properties of OAM have been widely studied [2], particularly for radio communication links where the orthogonality of different OAM modes suggest a novel multiplexing scheme [3–5].

In this work, we leverage the orthogonality of OAM radio waves to reduce crosstalk in adjacent antennas. The differential crosstalk created due to the OAM nature of the waves is measured and modeled. The result may be of interest in full-duplex communication links where it is desirable to transmit and receive simultaneously [6, 7]. OAM based crosstalk reduction can augment signal processing techniques and analog subtraction to achieve isolation between transmitter and receiver in full duplex systems [8–13]. Previous studies have shown good isolation between matched and mismatched OAM-based links for dual mode OAM antennas [7]. This work considers the crosstalk reduction between local transmitter and receiver, and its variation with the distance between them. A key finding in this work is the role of relative phase between the transmitting antenna and receiving antenna in OAM orthogonality based crosstalk reduction.

2. ANTENNA DESIGN, FABRICATION AND TEST

Several methods and devices have previously been used for the generation of OAM waves [5, 14–17]. In [18], phased array antennas were investigated and shown to produce OAM beams at 10 GHz. The

Received 25 February 2021, Accepted 8 May 2021, Scheduled 17 May 2021
* Corresponding author: Unaiza Tariq (utariq@smu.edu).
The authors are with the Electrical and Computer Engineering Department, Southern Methodist University, Dallas, TX 75275, USA.

same idea was extended herein to design a phased array antenna for the generation of OAM waves at 5.64 GHz. The antenna consists of a circular array of N patch antennas. To generate an OAM wave of mode l, the signal to each patch is phase shifted by $2\pi l/N$ radians from the adjacent patch [18].

The appropriate number of array elements has previously been studied. To avoid under-sampling, the number of antenna elements must satisfy $N > 2|l| + 1$ [18]. Therefore, to generate an OAM beam with mode *1*, the number of elements N must be greater than 3. In [18], a well-defined donut-shaped OAM with mode 1 is observed using $N = 8$. The same value of N has been used in our design. The array designed at 5.64 GHz is shown in Fig. 1. For $N = 8$, the signal to each patch must be phase shifted by $\pi/4$. To achieve this, a single signal is divided among 8 coaxial cables, each of which feeds 8 patches. The lengths of the coaxial cables are varied to create a difference in electrical length of $\pi/4$ between adjacent cables.

The array, designed to work at the operating frequency of 5.64 GHz, consists of 8 identical rectangular patch antennas, each with a length L of 13.12 mm and width W of 22 mm. The ANSYS High frequency simulation software (HFSS) is employed in the design process of the antenna array. A parametric analysis is carried out to determine the optimum value of array radius, which is found to be 34 mm. This is the radius at which the gain of the sidelobes of the OAM beam is found to be minimum.

The antennas were fabricated on Rogers RO4350B substrate material with a thickness of 0.762 mm using a ProtoMat S103 circuit board plotter. The RO4350B substrate has a dielectric constant of 3.66. Each patch antenna is fed using a coaxial cable connected using 50 Ω SMA female connectors. To generate OAM, the patches must be fired sequentially over the course of the RF cycle. This phase shift is achieved through a relative true time delay implemented in the 8 SMA cable lengths that feed the patches. Thus, the same signal is sent to each cable, but the length of the coaxial cable connected to each patch is varied to create a different phase shift in the signal reaching each patch. The difference in electrical length of each consecutive cable is $\pi/4$. Hence, the phase shift in signal goes from 0 (in the first patch) to $7\pi/4$ (in the last patch). Similarly, the order of the cables can be reversed to change the phase shift in the opposite direction from $7\pi/4$ to 0, and this reverses the mode of the OAM signal. The lengths of the cables are accurate up to 0.1 radians (or 6 degrees). At 5.64 GHz, the required time delay between adjacent patches is 22.16 ps, corresponding to a cable length difference of 4.388 mm.

The antenna is shown in a schematic and photograph in Fig. 1.

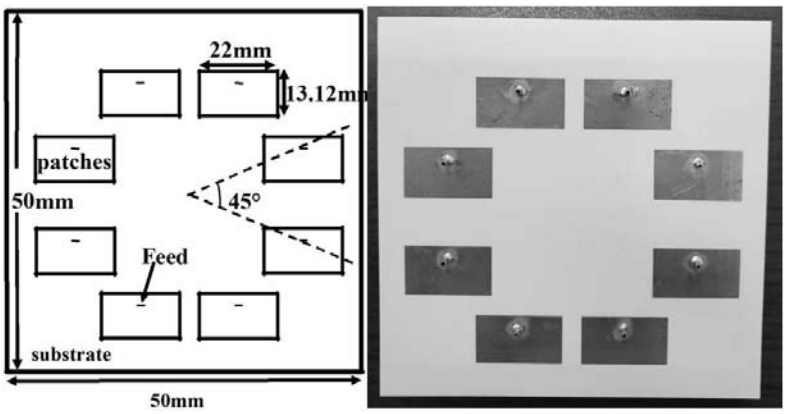

Figure 1. The schematic shows the design of the antenna for OAM generation at 5.64 GHz. The 45 degrees angle is both the physical measurement, and also the temporal phase measurement difference between patches excitation. The photograph shows the patch antenna array fabricated for OAM generation.

A single signal is split among the cables using an 8-way Wilkinson power divider (SP13856). The power divider has a nominal impedance of 50 Ω. It has SMA female connectors at input and output ports. If the inputs are given at the 8 output ports, the RF power divider can also be used as a power combiner, giving a combined output at the input port. The combiner configuration is used with the receiver antenna. The power divider/combiner has a nominal-theoretical loss of 9.03 dB. This causes

the signal to be significantly attenuated in the case of a transmitter, and in the case of receiver to be hardly perceptible.

An amplifier is connected before the Wilkinson divider to compensate for system losses. In the case of transmitter, a medium power GaAs amplifier has been used. It has a gain of 36 dB and P1 dB of 29 dBm. The amplifier has a constant gain over a frequency range of 60 MHz to 6 GHz. Three important precautions are taken in using the amplifier. 1. It is an ESD (electrostatic device) sensitive material, and it is therefore handled only on approved ESD workstations. 2. Heat sinks are employed to control the temperature of the amplifier, by cooling through conduction. 3. The amplifier is matched for 50 Ω loads and is a one-way device. Any impedance mismatch can cause reflected waves which can potentially damage the output stage of the amplifier. To avoid this, an isolator is connected at the output of the amplifier, to absorb any reflections. An RF isolator with 18 dB isolation is used.

The antenna design was simulated and analyzed using the ANSYS HFSS. A frequency analysis of a single patch of the array shows that resonance occurs at 5.64 GHz as shown in Fig. 2. The magnitude of the electric field distribution of the array, on a rectangular plane 60 mm away from the antenna, is seen to be a donut shape with a null in the center (Fig. 3). This null is characteristic of the shape of a radiation pattern with OAM.

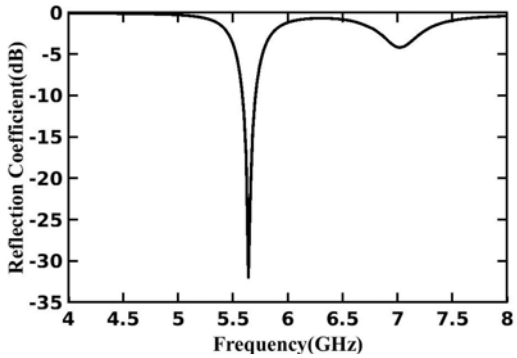

Figure 2. Reflection coefficient of a single patch of the array simulated in HFSS shows a resonance frequency of 5.64 GHz.

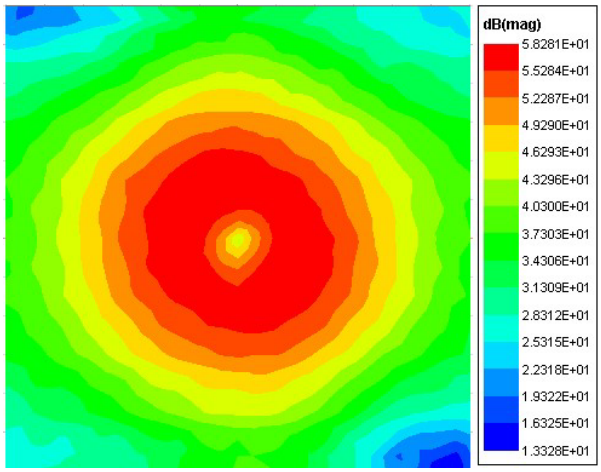

Figure 3. Magnitude plot of the electric field of the OAM wave calculated using HFSS, on a plane 60 mm away from the antenna.

The phase-front of an OAM signal is a rotating spiral shape. The rotation of the spiral phase front is determined by the OAM mode number. The clockwise rotation of the phase front shown in Fig. 4 is obtained for OAM mode $l = +1$. The mode can be changed to $l = -l$ by reversing the direction of the phases of each patch. This is done simply by reversing the sequence in which the cables are connected to the patches.

These results were verified in an anechoic chamber using the NFH007 Allwave antenna test system. The radiation pattern was determined to characterize the antenna. To further observe the phase pattern of the OAM beam, a 5.64 GHz waveguide probe receiver was moved in the x-y plane, at a distance of 86 inches in front of the OAM antenna. The phase pattern of the received signal was measured by the network analyzer and plotted by the Allwave software of the antenna test system. The phase pattern obtained, shown in Fig. 4(b) is distinctly a rotating phase-front, which is in good agreement with the simulated phase pattern shown in Fig. 4(a).

The radiation pattern, calculated by HFSS and measured by the network analyzer in the chamber, is plotted in Fig. 5, for $\varphi = 0$ and 90 degrees.

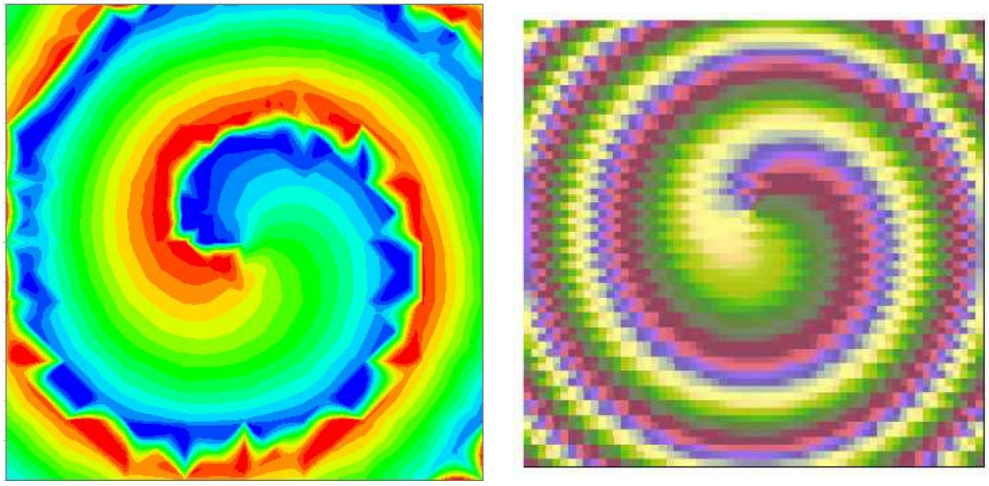

(a) (b)

Figure 4. (a) Simulated results for the phase pattern of the OAM antenna in the far field. (b) The phase pattern of the OAM antenna measured and plotted by the Allwave antenna testing system in an anechoic chamber. Both results confirm the rotating spiral phase front which is the signature of an OAM. In both figures the darkest shade represents 360 degrees and goes down to 0 degrees for the lightest shade.

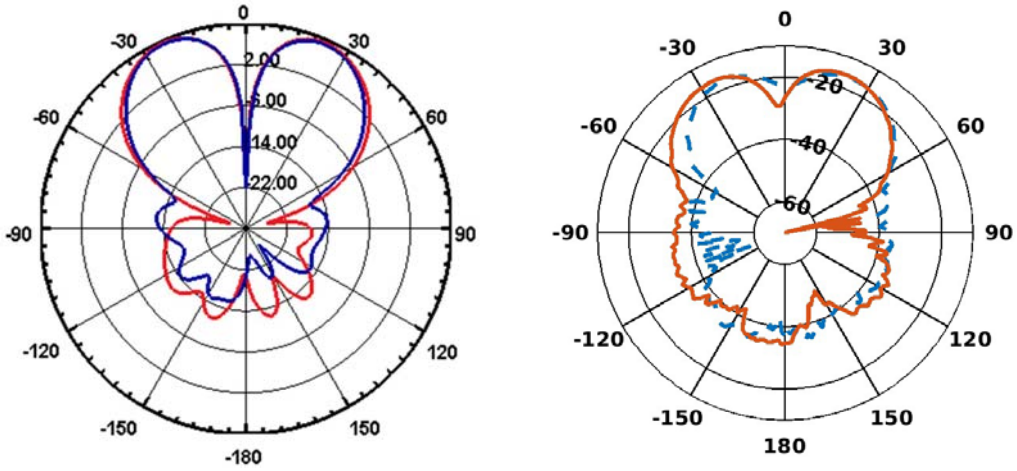

(a) (b)

Figure 5. The radiation pattern of the OAM antenna is obtained for the planes $\phi = 0$ and $\phi = 90$. (a) shows the simulated radiation pattern, (b) shows the pattern measured by the network analyzer of the Allwave antenna test system. In both figures, the red line represents the radiation pattern on the $\phi = 0$ plane, and the blue line represents the radiation pattern on the $\phi = 90$ plane.

3. CROSSTALK REDUCTION EXPERIMENTS

The signal captured by the receiver antenna is weak. To amplify the signal PAM-6000 high gain, benchtop preamplifier is used. It has a gain of 30 dB in the frequency range of 1 to 6 GHz. The maximum RF input is 2 dBm. The output of the Wilkinson combiner is directly connected to the input port of the PAM-6000 amplifier using a coaxial cable. The amplified signal from the output port is sent to the RF input port of the network analyzer.

All connections between the different parts of the RF system are made using coaxial cables. To

obtain accurate measurements, it is important not only for the performance of the antennas to be good, but also for the cables to be efficient. For this reason, ATC-PS test cable assemblies have been employed. These low loss 50 Ω coaxial cables are amplitude and phase stable over a frequency range of 0 to 20 GHz. The phase stability (with bending) of the cables is 5°, while the amplitude stability is 0.16 dB max.

The 8752C Network analyzer is used for the measurements. The network analyzer (NA) is operable over a frequency range of 300 kHz to 6 GHz. The network analyzer sends in a test signal to the transmitter network. The receiver network is connected to the input port of the network analyzer, to feed the received signal back into the network. The frequency range of the network analyzer is set from 2 GHz to 6 GHz. The network analyzer is used to measure the log magnitude of the signal transmitted from the transmitter to the receiver.

A block diagram showing the connections is given in Fig. 6. The transmitter and receiver arrays are held by wooden frames that are placed side by side as shown in Fig. 7. The distance between the antennas is measured from the edge of the transmitter array to the edge of the receiver array. When the antennas are placed adjacent to each other in this way, the log magnitude of the signal detected by the network analyzer is essentially the crosstalk measurement S_{12} between the transmitter and receiver. The experiment is carried out in a full anechoic chamber to exclude the effects of any reflected radiation, and to enhance the accuracy of the experiment.

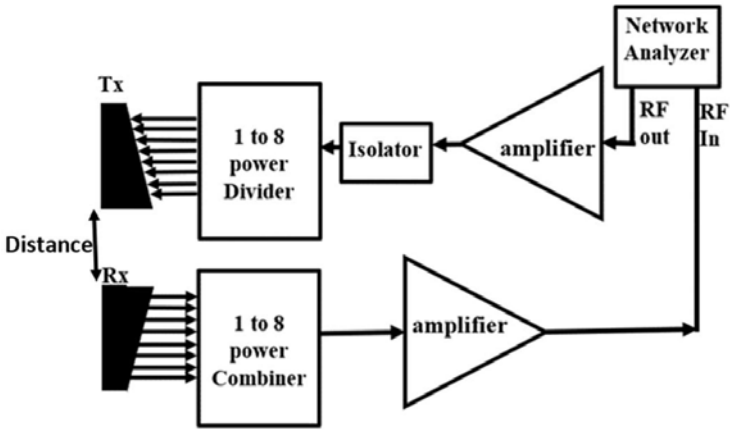

Figure 6. Block diagram of the setup for transmitter and receiver. The horizontal distance between the transmitter and receiver is varied.

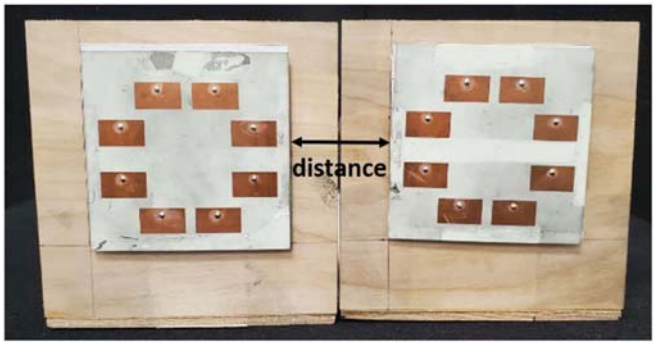

Figure 7. The transmitter and receiver antennas placed side by side. The horizontal distance between them is varied.

The horizontal distance between the two antennas is varied from 5.7 cm to 9.7 cm, in steps of 1 mm. For every distance, the S_{12} crosstalk measurement on the network analyzer is noted for the frequency of 5.64 GHz.

Increasing the horizontal distance between adjacent transmitter and receiver antennas would naturally vary the crosstalk value S_{12}. However, the objective of the experiment is to determine the additional crosstalk created due to the orthogonality of OAM modes, and to observe its variation with distance. Therefore, we must consider the difference between the S_{12} values when the two antennas have the same OAM modes and when they have opposite OAM modes, and calculate the difference between the crosstalk values to determine the differential or additional crosstalk that exists due to the OAM nature of the waves. For this purpose, the mode of the receiver is switched from $+l$ to $-l$ by reversing the sequence of the cables connected to the patches. The experiment is repeated for the opposite mode, and S_{12} values are again noted. Therefore, two cases have been studied,

i) transmitter mode $l_{Tx} = 1$, and receiver mode $l_{Rx} = 1$

ii) transmitter mode $l_{Tx} = 1$, and receiver mode $l_{Rx} = -1$

To see the effect of the mode of the OAM on the isolation, the difference between S_{12} values for the case of $l_{Rx} = 1$, $l_{Tx} = 1$ and the case of $l_{Rx} = -1$, $l_{Tx} = 1$ must be calculated. This value is the differential crosstalk ΔS_{12}.

Differential crosstalk, ΔS_{12}, is plotted against the horizontal distance between the transmitting and receiving antennas. The graph shows an oscillatory behavior of differential crosstalk ΔS_{12} with distance (Fig. 8).

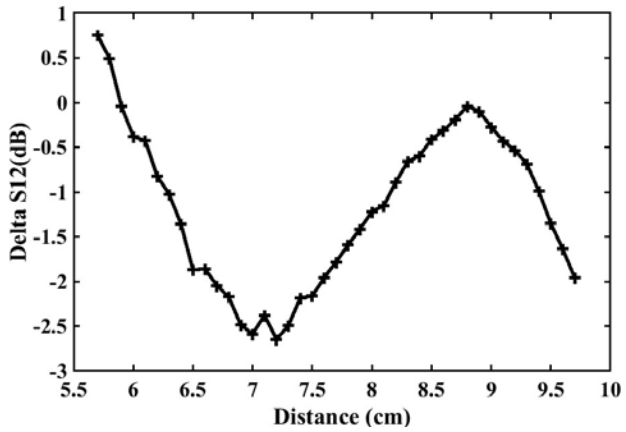

Figure 8. Variation of ΔS_{12} with distance between the antennas at 5.64 GHz.

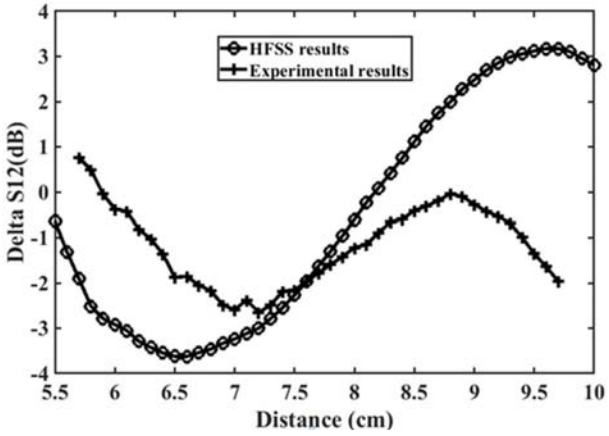

Figure 9. Comparison between the experimental and theoretical results for variation of differential crosstalk with distance between the antennas.

4. COMPARISON WITH THEORY

The experiment was also simulated in HFSS. Two patch arrays are similarly placed side by side with a distance D between them. A parametric analysis is run over distance D, and S_{12} is measured for both modes of receiver as discussed previously. Because of the limits of the precision of HFSS in this regime, multiple runs were averaged. The curves were filtered using the moving average filter to filter out the noise before averaging. The values of differential crosstalk ΔS_{12} are plotted against distance and compared with the plot obtained through practical measurements, in Fig. 9.

The sinusoidal variation of differential crosstalk ΔS_{12} with distance is evident from both plots. Despite differences between theory and experiment, a good match can be seen between the behavior of the experimental and simulated plots. All connections and components in the simulation are considered lossless. The simulation also uses ideal phase shifters to model the coaxial cables which have been used to provide phase shift to the patch antennas. In practice, there is a $\pm$6-degree error present in the phase shift provided by these cables. Moreover, the manual translation of the receiver away from the transmitter contributes human error to the experiment.

5. CONCLUSION

The oscillatory character of ΔS_{12} with distance provides insight into the nature of the effect. OAM orthogonality based crosstalk reduction between a transmitting antenna and a receiving antenna stems from the role of relative phase between the two antennas. We further postulate that the disturbances on the quiescent, receiving antenna combine coherently in accordance with the relative phase shifts provided by the SMA cables that feed the two antennas. Thus, the disturbances on the patches of the receiving antenna add constructively or destructively depending on the distance dependent propagation delay between the two antennas.

The isolation studied here is achieved due to OAM orthogonality and is in addition to the isolation due to the separation of the antennas. At present, the reduced differential crosstalk between transmitter and receiver is modest. The theoretical analysis predicts a maximum isolation of 3.6 dB, and in the experiments, the prototype realizes 2.6 dB of maximal reduced crosstalk. This work may, however, promote investigations of alternate geometries that may provide improved crosstalk reduction.

ACKNOWLEDGMENT

The authors greatly appreciate advice and consultation from Professor Rashaunda Henderson at The University of Texas at Dallas. We would also like to thank Mr. Scott McWilliams for his help in the biotechnology lab at the Southern Methodist University, Dallas, where the antennas were fabricated. The authors have benefited as well from conversations with Dr. Solyman Ashrafi at NxGen. U. Tariq also thanks Ms. Maira Islam from National University of Sciences and Technology, Pakistan for sharing her knowledge of HFSS.

REFERENCES

1. Allen, L., M. W. Beijersbergen, R. J. C. Spreeuw, and J. P. Woerdman, "Orbital angular momentum of light and the transformation of Laguerre-Gaussian laser modes," *Phys. Rev. A*, Vol. 45, No. 11, 8185–8189, Jun. 1992. Accessed on: Sep. 7, 2020, doi: 10.1103.PhysRevA.45.8185, [Online].
2. Yao, A. M. and M. J. Padgett, "Orbital angular momentum: Origins, behavior and applications," *Adv. Opt. Photonics*, Vol. 3, No. 2, 161–204, May 2011. Accessed on: Sep. 7, 2020, doi: 10.1364.AOP.3.000161, [Online].
3. Tamburini, F., E. Mari, A. Sponselli, B. Thidé, A. Bianchini, and F. Romanato, "Encoding many channels on the same frequency through radio vorticity: First experimental test," *New J. Phys.*, Vol. 14, No. 3, 3001–3018, Mar. 2012. Accessed on: Sep. 11, 2012, doi: 10.1088.1367.2630.14.3.03001, [Online].
4. Tamburini, F., E. Mari, G. Parisi, F. Spinello, M. Oldoni, R. A. Ravanelli, P. Coassini, C. G. Someda, B. Thidé, and F. Romanato, "Tripling the capacity of a point-to-point radio link by using electromagnetic vortices," *Radio Sci.*, Vol. 50, No. 6, 501–508, Jun. 2015. Accessed on: Sep. 7, 2020, doi: 10.1002.2015RS.005662, [Online].
5. Spinello, F., E. Mari, M. Oldoni, R. A. Ravanelli, C. G. Someda, F. Tamburini, F. Romanato, P. Coassini, and G. Parisi, "Experimental near field OAM-based communication with circular patch array," *Optics*, 1507.06889, Jul. 2015.
6. Ashrafi, S., "Full duplex using OAM," Patent 20200044349, [Online]. Available: Justia: Patents: US Patent Application for FULL DUPLEX USING OAM Patent Application.
7. Zhang, Y. and J. Li, "Analyses and full-duplex applications of circularly polarized OAM arrays using sequentially rotated configuration," *IEEE Transactions on Antennas and Propagation*, Vol. 66, No. 12, 7010–7020, Dec. 2018, doi: 10.1109/TAP.2018.2872169.
8. Choi, J. I., M. Jain, K. Srinivasan, P. Levis, and S. Katti, "Achieving single channel, full duplex wireless communication," *International Conference on Mobile Computing and Networking*, 2010, [Online], available: https://web.stanford.edu/∼skatti/pubs/mobicom10-fd.pdf.

9. Chen, S., M. Beach, and J. McGeehan, "Division-free duplex for wireless applications," *IEEE Electron. Lett.*, Vol. 34, No. 2, 147–148, Jan. 1998. Accessed on: Sept. 6, 2020, doi: 10.1049/el:19980022.
10. Duarte, M., "Full-duplex wireless: Design, implementation and characterization," PhD. Dissertation, Rice Univ., Houston, Tx, 2012.
11. Duarte, M., A. Sabharwal, V. Aggarwal, R. Janna, K. K. Ramakrishnan, C. W. Rice, and N. Shankaranarayanan, "Design and characterization of a full-duplex multiantenna system for WiFi networks," *IEEE Trans. Veh. Technol.*, Vol. 63, No. 3, 1160–1177, Mar. 2012. Accessed on: Sep. 7, 2020, doi: 10.1109.TVT.2013.2284712, [Online].
12. Jain, M., J. I. Choi, T. Kim, D. Bharadia, S. Seth, K. Srinivasan, P. Levis, S. Katti, and P. Sinha, "Practical, real-time, full duplex wireless," *MobiCom*, Las Vegas, Nevada, USA, Sep. 19–23, 2011.
13. Sahai, A., G. Patel, C. Dick, and A. Sabharwal, "On the impact of phase noise on active cancellation in wireless full-duplex," *IEEE Trans. Veh. Technol.*, Vol. 62, No. 9, 4494–4510, Nov. 2013. Accessed on: Sep. 7, 2020, doi: 10.1109.TVT.2013.2266359, [Online].
14. Trinder, J. R., "Parabolic reflector," Patent WO 2005069443, Jul. 28, 2005.
15. Schemmel, P., G. Pisano, and B. Maffei, "Modular spiral phase plate design for orbital angular momentum generation at millimetre wavelengths," *Opt. Express*, Vol. 22, No. 12, 14712–14726, Jun. 2014. Accessed on: Sep. 8, 2020, doi: 10.1364.OE.22.014712, [Online].
16. Gao, X., S. Huang, J. Zhou, Y. Wei, C. Gao, X. Zhang, and W. Gu, "Generating, multiplexing/demultiplexing and receiving the orbital angular momentum of radio frequency signals using an optical true time delay unit," *J. Opt.*, Vol. 15, No. 10, 5401–5407, Aug. 2013. Accessed on: Sep. 8, 2020, doi: 10.1088.2040.8978.15.10.105401, [Online].
17. Mahmouli, F. E. and S. Walker, "Orbital angular momentum generation in a 60 GHz wireless radio channel," *20th TELFOR*, Nov. 2012, [Online]. Available: https://ieeexplore.ieee.org/document/6419210.
18. Bai, Q., A. Tennant, and B. Allen, "Experimental circular phased array for generating OAM radio beams," *Electron. Lett.*, Vol. 50, No. 20, 1414–1415, Sep. 2014. Accessed on: Sep. 8, 2020, doi: 10.1049.el.2014.2860, [Online].